Chitosan/glycosaminoglycan scaffolds for skin reparation

Giuseppina Sandri[1,*], Silvia Rossi[1], Maria Cristina Bonferoni[1], Dalila Miele[1], Angela Faccendini[1], Elena Del Favero[2], Emanuela Di Cola[2], Antonia Icaro Cornaglia[3], Cinzia Boselli[1], Thomas Luxbacher[4], Lorenzo Malavasi[5], Laura Cantu'[2,*], Franca Ferrari[1]

[1]Department of Drug Sciences, University of Pavia, Viale Taramelli 12, 27100 Pavia, Italy

[2]Department of Medical Biotechnology and Translational Medicine, University of Milano, LITA, Via Fratelli Cervi 93, 20090 Segrate (Milano) Italy

[3]Department of Public Health, Experimental and Forensic Medicine, University of Pavia, via Forlanini 2, 27100 Pavia, Italy

[4]Anton Paar GmbH, Anton-Paar-Str, 20 8054 Graz, Austria

[5]Department of Chemistry, University of Pavia, Viale Taramelli 14, 27100 Pavia, Italy

*Corresponding authors:

Prof. Giuseppina Sandri

Department of Drug Sciences,

University of Pavia,

Viale Taramelli 12, 27100 Pavia, Italy

giuseppina.sandri@unipv.it

Prof. Cantu' Laura

Department of Medical Biotechnology and Translational Medicine

University of Milano

LITA, Via Fratelli Cervi 93, 20090 Segrate, Italy

laura.cantu@unimi.it

ABSTRACT

Burns and chronic wounds, often related to chronic diseases (as diabetes and cancer), are challenging lesions, difficult to heal. The prompt and full reconstitution of a functional skin is at the basis of the development of biopolymer-based scaffolds, representing a 3D substrate mimicking the dermal extracellular matrix. Aim of the work was to develop scaffolds intended for skin regeneration, according to: fabrication by electrospinning from aqueous polysaccharide solutions; prompt and easy treatment to obtain scaffolds insoluble in aqueous fluids; best performance in supporting wound healing. Three formulations were tested, based on chitosan (CH) and pullulan (P), associated with glycosaminoglycans (chondroitin sulfate - CS or hyaluronic acid – HA). A multidisciplinary approach has been used: chemico-physical characterization and preclinical evaluation allowed to obtain integrated information. This supports that CS gives distinctive properties and optimal features to the scaffold structure for promoting cell proliferation leading tissue reparation towards a complete skin restore.

Keywords: electrospinning, chitosan, glycosaminoglycans, chronic wound and burn healing, in vitro and in vivo models

1. INTRODUCTION

Millions of people in the world suffer from chronic skin lesions. These are challenging and are affected by an intrinsic inability to heal. Cellular and molecular abnormalities occurring at wound bed, including phenotypic aberrations and perturbations of ECM microenvironment, significantly alter the normal recovery phases, leading to a possible impairment of the healing path and finally to non-healing wounds. Moreover, among skin wounds, burns require special attention because often prone to infections and to abnormal scarring (Mafazzal Jahromi et al., 2018).

Because of the crucial barrier role of the skin, chronic wounds (including venous leg ulcers, diabetic foot ulcers, arterial insufficiency and pressure ulcers) and burns impose substantial morbidity and mortality. They deeply affect the quality of life of patients, with high economic burden (Stejskalova, Almquist, 2017).

Wound healing can be enhanced by tissue engineering: in particular, the use of scaffolds promotes the formation of a defined biomimetic environment surrounding cells to allow cell-cell specific interactions (Goldberg, Langer, Jia, 2012). The structure and morphology of the ECM of skin dermis can be easily resembled by nanofibrous structures, reported as ideal constructs to enhance cell adhesion and proliferation (Liu et al., 2017). Uniform and continuous nanofibers are easily obtained by means of electrospinning as a simple, flexible and versatile method.

Given these premises, the aim of this work was the development of electrospun nanofibrous scaffolds based on glycosaminoglycans, either chondroitin sulfate (CS) or hyaluronic acid (HA), and chitosan (CH), to enhance cutaneous wound healing of chronic lesions and burns.

Glycosaminoglycans (GAGs) have been selected as important components of ECM and play a crucial role in different stages of skin tissue regeneration and maturation. In particular CS, a structural component of ECM (Oliveira, Reis, 2011) is able to interact with positively charged bioactive molecules, in particular growth factors (GF) and is reported as effective enhancer of cell proliferation (Sandri et al., 2012; Sandri et al., 2015; Sandri et al., 2016; Saporito et al., 2018). Analogously, HA plays pivotal roles in regulating proliferation, migration, cell differentiation and angiogenesis (Kin et al., 2017).

Moreover CH has been selected as enabling polymer characterized by bioadhesion, biocompatibility, biodegradability, antimicrobial activity, and wound healing properties (Liu et al., 2018).

However polysaccharides, in general, and CH, in particular, are hardly spinnable and CH nanofibers are usually obtained starting from organic solution (i.e. trifluoacetic acid and hexa-fluoro isopropanol) that could leave highly toxic traces or by blending chitosan with easily spinnable synthetic polymers (as poly(ethylene oxide) or poly(vinyl alcohol) (Qasim et al., 2018).

In the present work, CH was associated to pullulan (P), an easily spinnable polysaccharide having numerous food, pharmaceutical and biomedical application (Singh et al., 2017). The preparation was robust with a one step process and easy to set up. An aqueous/acetic acid medium was used to avoid toxic residues and to allow the electrospinning of polymers having opposite charges (CH cationic and GAG anionic). Moreover, citric acid (CA) was used as crosslinker and a thermal treatment was applied to render the scaffold insoluble in aqueous environment. A multidisciplinary approach, involving chemico-physical and preclinical evaluation, has been used to characterize the scaffolds.

2. EXPERIMENTAL SECTION

2.1 Materials

Chitosan (CH) (charge density - positive = 0.006 mol/g), Chondroitin sodium sulfate (CS) (charge density - negative = 0.002 mol/g), Hyaluronic Acid (HA) (charge density - negative = 0.0013 mol/g) Pullulan (P) and citric acid (CA) (charge density - negative = 0.014 mol/g) were used (details summarized in supplementary information (SI), Fig. S1).

2.2. Methods

2.2.1. Preparation of polymeric blends and characterizations

All the polymeric blends were based on P, CH and CA, as such or containing CS or HA. P solution was prepared in distilled water and CS or HA were added to P, thus preparing three different solutions: P; P/CS P/HA. CH was hydrated in acetic acid (90% v/v) and citric acid was added. Three different polymeric blends were prepared by mixing each P, P/CS, and P/HA with CH solution at 1:1 weight ratio. The following blends were prepared (w/w): CH, CH/CS and CH/HA. The role of acetic acid was fundamental to reduce blend surface tension and allow their electrospinning. The blends composition is reported in Table 1.

Table 1: composition (% w/w) of polymeric blends used to be elctrospun for scaffolds construction. In the brackets the relative charge density per each component is reported.

% w/w	P	CH	CA	CS	HA	Water/acetic acid
CH	10	2.5 (+0.0015)	2.5 (-0.01)	--	--	55/45
CH/CS	10	2.5 (+0.0015)	2.5 (-0.01)	0.5 (-0.001)	--	55/45
CH/HA	10	2.5 (+0.0015)	2.5 (-0.01)	--	0.5 (-0.00065)	55/45

2.2.2. Physical properties of polymeric blends

The viscosity of CH, CH/CS and CH/HA blends was assessed by a rotational rheometer (Rheostress 600, Haake, Enco, I), in the cone-plate configuration (C35/1: diameter= 35mm; cone angle= 1°), rest time = 3 min, shear rate = 100 s^{-1}, T=25°C,

The surface tension of the blends was measured at T=32°C with a tensiometer (DY-300, Kyowa, J) (measurement range 0-100 mN/m) and their electrical conductivity was determined by a conductometer (FiveGoTM - Mettler Toledo, I).

2.2.3 Preparation of electrospun scaffolds

Scaffolds were obtained from the CH, CH/CS and CH/HA blends using an electrospinning apparatus (STKIT-40, Linari Engineering, I), equipped with a high-voltage power supply (Razel R99-E 40, kV), a 10 ml syringe with 21G needle (0.8x20 mm), and a conductive static collector, covered by an aluminum foil. The following parameters were used: ΔV (voltage) = 21 kV (CH) or 15 kV (CH/CS and CH/HA), needle-to-collector distance = 20 cm (CH) or 15 cm (CH/CS and CH/HA), polymeric solution flux = 0.4 ml/h, spinning time = 1 h. The obtained CH, CH/CS and CH/HA scaffolds were then crosslinked by heating at 150°C for 1 h. This process is also reported as able to dry sterilize the products (Kupiec et al., 2000).

2.2.3.1. Scaffold chemico-physical characterization

Scaffold morphology was analyzed by means of SEM (Tescan, Mira3XMU, CISRIC, University of Pavia) after graphite sputtering. The scaffolds were analyzed before and after the crosslinking procedure and after 1-week of hydration in distilled water. Nanofiber diameters were determined by an image analysis software (Image J, ICY, Institute Pasteur, F).

FT-IR analysis was carried out by means of Infrared Imaging Microscope (Nicolet iN10 MX, Thermo Scientific). The infrared spectra were acquired in the range 4000-500 cm^{-1} (tested area 10-20 μm^2).

2.2.3.2. Structural characterization

X-ray scattering experiments were performed at the high-brilliance ID02 beamline at ESRF (Grenoble, France) in the q-ranges $0.007 \leq q \leq 5$ nm^{-1} (SAXS, mesoscale structure determination) and 15-30 nm^{-1} (WAXS, local lengthscale organization). Small pieces (~1 cm^2) were cut from the different scaffolds, both before and after crosslinking. Cuts of the crosslinked membranes were dipped in distilled water or NaCl 156 mM solution 24 h before measurement. Both dry and wet samples were loaded in plastic capillaries 2 mm

thick (KI-beam, ENKI) and placed in front of the X-ray beam (Fig. S2a in SI). During data reduction, cell contributions were subtracted from the measured spectra.

2.2.3.3 Calorimetry.

Small portions of different dry membranes (ranging 7-8 mg) either crosslinked or not, were adapted to calibrated aluminum crucibles, then weighted. Crucibles were put into a solid state calorimeter (DSC131, Setaram, FR), under nitrogen atmosphere, then submitted to subsequent temperature heating/cooling scans at 2 °C/min or 10 °C/min scan rate in the temperature range 30-180°C, to test for process reversibility and reproducibility. For the non-crosslinked samples, the first heating scan was limited to 150°C, then followed by 1h-isothermal equilibration at 150°C, similarly to the crosslinking protocol. Samples were equilibrated for 30 min at the extreme temperatures in between the subsequent scans. The background contribution of void crucible was measured for subtraction and calibration.

2.2.3.4. Surface zeta potential

The apparent zeta potential (ζ) of each scaffold was determined from the measurement of the streaming potential. Also, the streaming current was measured to estimate the extent of scaffold swelling affecting the overall conductivity (see SI). Streaming potential measurements were performed with SurPASS™ 3 (Anton Paar GmbH, Austria) using the clamping cell (Walker et al., 2002). The scaffolds (17x17 mm^2, active area 10x10 mm^2) were mounted dry opposite to a reference surface (Figure S3a, SI).

10 mM KCl aqueous solution was used as the streaming solvent and its pH was scanned in the range 2.5-9, to determine the isoelectric point (iep) and the ζ at physiological pH.

The ζ was calculated from streaming potential and streaming current measurements using the equations by Helmholtz and von Smoluchowski (Luxbacher, 2014), as detailed in the SI. The contribution of the reference material to the ζ of the scaffolds was estimated as negligible and the pH dependence of the ζ for these rigid, non-porous, non-conductive materials is shown in SI (Fig. S3b).

2.2.3.5. Mechanical properties

Dried or hydrated scaffolds were subjected to tensile measurements by means of a TA.XT plus apparatus (Stable Microsystems, ENCO, Italy), as briefly described in SI (Saporito et al., 2018a). The ratio between the increase in the distance of the two grips at scaffold breaking and the initial one was then expressed in terms of percent elongation of the scaffold, namely, $E\% = 100x(L_{fin}-L_{in})/L_{in}$.

2.2.3.6. In vitro cells adhesion and proliferation assay

Adhesion and proliferation assays were carried out using two cell lines: fibroblasts (normal human dermal fibroblasts (NHDF from juvenile foreskin, PromoCell, WVR, Italy) and endothelial cells from human umbilical vein (HUVEC, Lonza, Italy), as briefly described in SI (Saporito et al., 2018a).

Scaffolds were cut to have a final area of 0.36 cm^2 (0.7 cm diameter) to cover the bottom of a 96 well-plate and both cell types were seeded onto each scaffold at 10^5 cells/cm^2 seeding density and grown for 3 and 6 days. Cells grown in standard conditions were considered as control (GM). After 3 or 6 days of growth, MTT assay (as briefly described in SI (Sandri et al., 2017)), SEM and CLSM analysis (as briefly described in SI (Saporito et al., 2018a)) were performed.

2.2.3.7. In vivo wound healing efficacy in murine burn/excisional model

All animal experiments were carried out in full compliance with the standard international ethical guidelines (European Communities Council Directive 86/609/EEC) approved by Italian Health Ministry (D.L. 116/92). The protocol is briefly reported in SI (Sandri et al., 2017). CH, CH/CS or CH/HA scaffolds having 4 mm diameter as the lesions were applied and wetted with 20 μl of saline solution (0.9 g/l). Size of wounded area and the histology of biopsies were performed, as briefly described in SI (Sandri et al., 2017).

2.2.3.8. Statistical analysis

Statistical differences were evaluated by means of a non-parametric test: Mann Whitney (Wilcolxon) W test, (Statgraphics Centurion XV, Statistical Graphics Corporation, MD, USA). Differences were considered significant at $p<0.05$.

3. Results and discussion

3.1. Physical properties of polymeric blends

The addition of CH-CA, alone and with CS or HA, significantly increased (~ one order of magnitude) the viscosity of the solution as compared to pure P, as expected for molecular complexation. Then, the viscosity values of the various blends are similar (within 3%), the smallest being that of CH/CS, compatible with a more pronounced charge unbalance due to CS. The values of surface tension are almost similar for all blends, the one of CH/CS being the lowest, again compatible with a more pronounced overall charge. Accordingly, conductivity decreases in the series CH/CS>CH>CH/HA, with an overall span of ~20%. In fact

conductivity is directly related to the particle concentration and mobility in the solution. Unbalanced particle charge density generally increases with the conductivity, influencing fiber diameter during electrospinning (Huan et al., 2015). Table S1 (SI) reports the viscosity, surface tension and conductivity of the polymeric blends used to prepare the scaffolds.

3.2. Scaffold chemico-physical and structural characterization

Different physico-chemical techniques were applied to assess the morphology and structure of the scaffolds on different lengthscales. Besides the characterization of the final membranes, the effect of crosslinking was addressed. In fact, while non-crosslinked membranes readily dissolve in contact with water, crosslinking made them stable against solubilization. Moreover, the extent of scaffold stability was inspected by delayed testing, as detailed in the following.

3.2.1. Fiber morphology

Figure 1 reports SEM microphotographs of nanofibrous scaffolds 1) immediately after preparation (not crosslinked, NC, left), 2) after cross-linking (center) and 3) dried after 6 days immersion in water (right). For all the compositions, nanofibers show regular shape and smooth surface and the cross-linking process does not change their morphology. The regular and smooth appearance of nanofibers is preserved upon 6-days hydration, although they show up to be stuck to each other.

The fibers cross section seems not to be altered upon crosslinking, being in the range of 500 nm in diameter, nor they break in shorter tracts. In the CH scaffold the nanofibers are slightly thinner. Hydration causes a slight swelling of the nanofibers, more evident in the CH scaffold and negligible in CH/CS. The wet fibers morphology suggests that water penetration within the structure is not prevented for any of the compositions, but that especially the CH/CS scaffold is more resistant against the fiber swelling deformation.

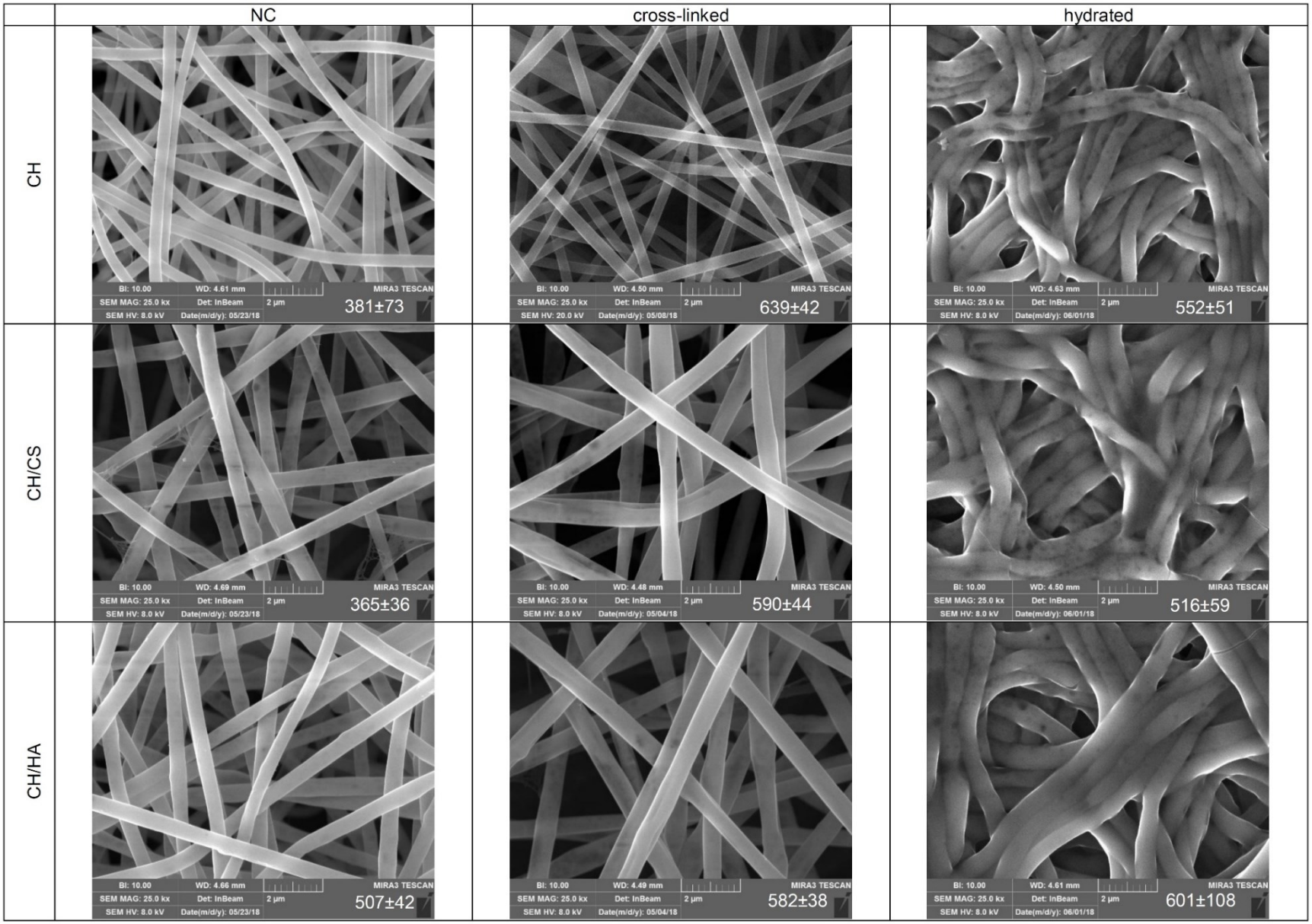

FIGURE 1: SEM microphotographs of scaffolds immediately after preparation (not crosslinked, NC), after cross-linking and after 6 days hydration in water. In each image the diameters (nm) are reported (mean values±sd; n=100) (Mann-Whitney – Wilcoxon: CH= NC vs hydrated: p=0.002; cross-linked vs hydrated: p=0.005; CH/HA: cross-linked vs hydrated: p=0.037; cross-linked: CH vs CH/CS: p=0.005; CH vs CH/HA: p=0.001; CH/CS vs CH/HA: p=0.018; hydrated: CH vs CH/CS: p=0.017; CH vs CH/HA: p=0.039)

241 Since, during the electrospinning and the subsequent crosslinking process, acetic acid volatizes, it is
242 conceivable that anionic and cationic moieties could interact during this phase. Considering that CS is an
243 acid stronger than HA (pKa CS: 1.5-2; HA: 2.87), a tighter and stronger anionic/cationic interaction between
244 CS and CH could be at the basis of this behavior, although, in all systems, P forms mass-predominant
245 neutral matrix in a network formed by the interacting charged components with a clear excess of negative
246 charges (Table 1). It is conceivable that CH and CS or HA interacted forming polyelectrolyte complexes
247 (PEC) (Saporito et al., 2018b) and PEC could also occur, mediated by the CA macroion as crosslinker, since
248 CH polycation and CA multivalent macro-anion are present in the same weight fraction. The tuning
249 contribution coming from either HA or CS polyanions, present in lower amount in the corresponding
250 scaffolds, causes significant differences in swelling behavior.
251
252 3.2.2. FTIR characterization.
253 Figure 2 reports the FTIR profiles of the three scaffolds before and after crosslinking, giving a fiber local
254 response to crosslinking. Overall, the spectra are in agreement with current literature where the specific peak
255 assignment can be found (Harish Prashanth, Kittur and Tharanathan, 2002; Feng, Liu, Zhao and Hu, 2012).
256 As for CH scaffold, a significative effect following crosslinking is present in the region around 1640 cm^{-1},
257 typical of the Amide I band, that could be related to covalent bonds occurring between chitosan aminogroups
258 and carboxylic moieties of citric acid. For the two scaffolds CH/CS and CH/HA, differences are less marked
259 and only slight variations could be seen, again, in the region of Amide I band, suggesting that the presence
260 of anionic groups from CS (sulfate) and HA (carboxylic) and polymer steric hindrance could tune covalent
261 bond formation between CH and CA.

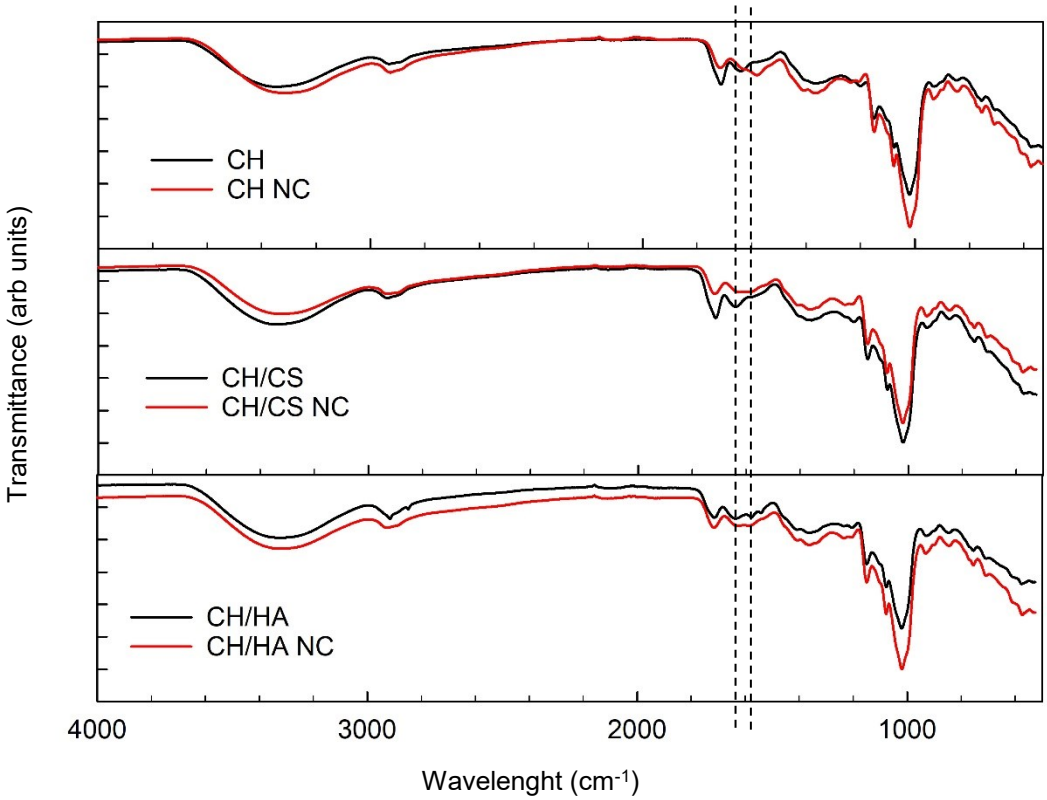

FIGURE 2: FTIR profiles for CH, CH/CS and CH/HA scaffolds, not crosslinked (NC) and crosslinked. A vertical dashed line is drawn in the region of the Amide I band.

3.2.3. Structural characterization

X-ray scattering measurements allow to access the structural features of the membranes from the mesoscale (SAXS, up to hundreds of nm) to the local arrangement (WAXS, down to tenth of nm), thus integrating the SEM morphological observation in revealing intra-fiber and inter-fiber structure, whether structural modification follow crosslinking, and hydration and aging effects. WAXS spectra in dry state does not display any feature for any of the membranes in any condition, thus showing that the electrospun blend fibers are not built by stacking or piling of elements but by randomly arranged complexed polymer chains. The SAXS spectra (I(q) versus q) are plotted in Figure 3 (A) in the whole SAXS range, vertically shifted for better visibility.

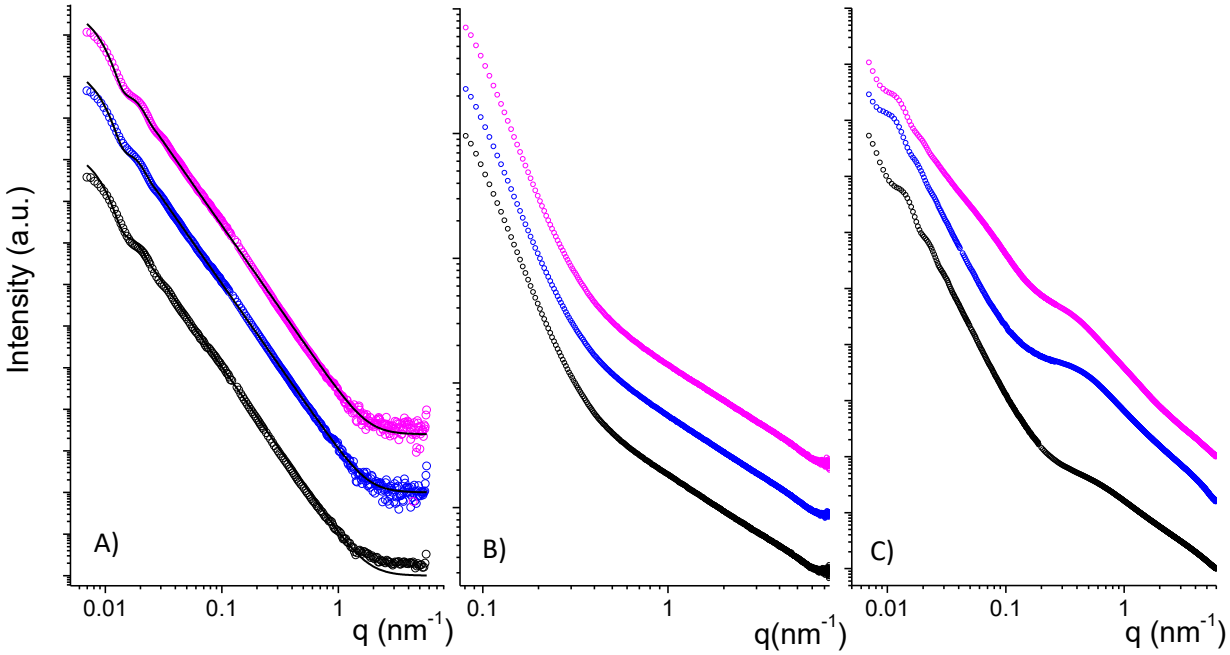

FIGURE 3. A) SAXS spectra of the dry crosslinked membranes (top violet: CH/CS; centre blue: CH/HA; bottom black: CH). The fitting curves are shown. The (q^{-4})-slope is observed over more than two decades. B) SAXS spectra of the crosslinked membranes after 24h immersion in DDH_2O, in the q-range corresponding to the d<100 nm lengthscale (top: CH/CS; centre: CH/HA; bottom: CH). The transition from the low-q slope (q^{-4}, see left panel) and the q^{-1} regime is clearly visible. C) SAXS spectra of the crosslinked membranes after 4-months aging in DDH_2O, in the same q-range of left panel (top: CH/CS; centre: CH/HA; bottom: CH). Spectra are shifted for better visibility.

The spectra are very similar and can be fitted with the form factor of uniform infinitely long cylinders (Pedersen, 1997) with moderate polydispersity (15%-20%), with average cross size of ~500 nm, compatible with the SEM observations, accounting for the variability of sample preparations. An interesting feature is that a (q^{-4})-slope is observed for all membranes over a large q-range, covering the micro-to-nanoscale, typical of objects with smooth surface. Spectra from the non-crosslinked membranes are very similar to their crosslinked analogs, indicating similar size and surface smoothness of the nanofibers (Figure S2b in SI). SAXS measurements were also performed on wet scaffolds, after 24 h immersion in distilled water. No difference is detected upon salt addition. All spectra show a clear deviation from the steep decay starting at q ~ $3x10^{-1}$ nm^{-1}, corresponding to a typical distance of ~ 20nm, as shown in Figure 3 (B). The slope in this second regime is that of (q^{-1}), revealing the presence of additional structures on much smaller lenghscales than the fiber cross-section, with elongated shape. Those structures are conceivably polymer chains protruding and stretching out from the fibers surface.

SAXS measurements were then repeated on the same membranes after 4-months aging in wet environment, to check for membrane structure evolution, reported in Fig. 3 (C). The three scaffolds

underwent different processes: the structure of the naked CH scaffold is preserved on both the long-range and the local length-scales. The slight swelling of the fiber cross-size (~20%) indicated that hydration occurred, as expected upon membrane immersion into aqueous medium, still the fibers do not unwrap or disentangle or loose polymer chains. The CH/HA scaffold, instead, undergoes some structure alterations, as evident from the rise of a clear shoulder in the high-q region of the spectrum, the low-q region being unchanged and very similar to that of the naked CH scaffold. The shoulder could be reproduced by adding a contribution coming from gaussian chains with gyration radius of 4 nm (see Fig.S2C in SI). This suggests that, upon aging, longer HA chains portions (~10 monomers) protrude from the main structure, assuming a coiled conformation. The deepest aging structural modification occurs in the CH/CS scaffold, (Fig. 3, C) that displays changes in all the q-range. The appearance of the high-q shoulder is paralleled by a reduction of the low-q slope from q^{-4} to $q^{-2.8}$, typical for a fractal structure. This is related to a more pronounced surface roughening of the fibers. It seems that fibers might lose more easily some CS chains (shorter and highly charged than HA and CH) probably wrapped and not intimately woven within the fibers.

No differences could be highlighted after scaffold hydration in NaCl 156 mM.

3.2.4. Calorimetry

Calorimetry measurements were performed on non-crosslinked and crosslinked dry scaffolds, simulating the cross-linking process by suddenly raising the temperature of the non-crosslinked electrospun scaffolds from room up to 150°C, followed by 1-hour annealing.

The DSC profiles obtained with a high scan-rate (10°C/min) on non-crosslinked samples are shown in Figure 4. All profiles display the water-release endothermic peak (Yamaguci et al., 2001) completing below the annealing temperature. The corresponding enthalpies, normalized by the sample mass to give the water-holding capacity, are 244 J/g (CH), 299 J/g (CH/CS) and 279 J/g (CH/HA). The subsequent cooling to room temperature and the repeated cycles are relative to annealed scaffolds in DSC-crosslinking simulated protocol. No exothermic peak in the cooling scans is detected in the investigated range (Fig. 4) and no water-release peak is observed in the following heating scans. Rather, the water-release peak is again observed in the first DSC heating scan performed on the same samples after some delay (two weeks, two and four months), showing that the scaffolds recover their hydration level in time.

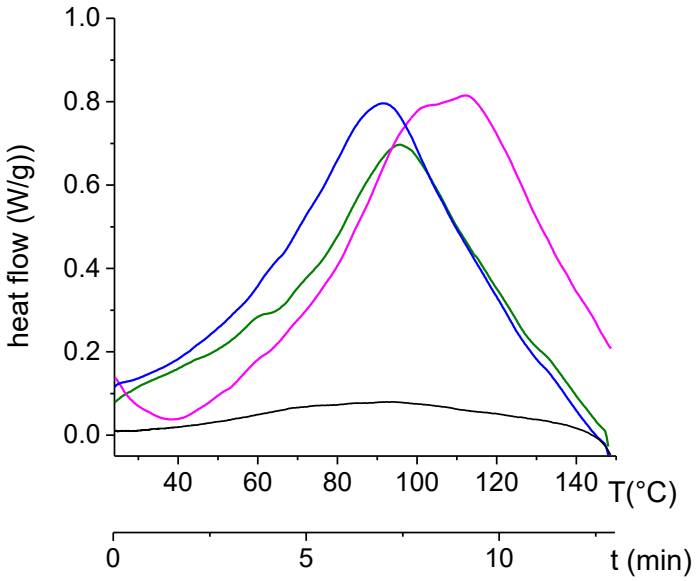

FIGURE 4. DSC-crosslinking simulation on different scaffolds with a fast (10°C/min) heating from room temperature to 150°C, of the CH (green) CH/HA (blue) and CH/CS (violet) scaffolds. In black a representative of a cooling scan. Below the temperature axis, the time axis is drawn.

Similar peaks are present in the calorigrams of the constituent materials, disappearing on closely subsequent scans and reappearing upon exposure to ambient humidity, indicating their relation to hydration. Moreover (Fig S3a in SI) the relative positions of the water-release peaks of the different scaffolds reflect the ones of their components.

DSC profiles of the originally-crosslinked membranes, performed at a lower scan rate of 2°C/min, are reported in Fig.5 (A). Again, the water-release peak can be clearly observed in the first heating, while it is never found in the following runs within the same experiment, as before, indicating the water-holding capacity is preserved upon crosslinking. Moreover, DSC profiles of DSC-simulated crosslinked samples (Fig.4, after two weeks), performed with the lower scan-rate of 2°C/min and shown in Fig.5 B for direct comparison, are very similar to those in left panel, stemming for good reproducibility over different samples and basic features of crosslinking. In general, the crosslinking procedure results in a downshift of the water-release temperature by ~5°C, as shown in Fig.5 C for the CH matrix, and in a higher water-holding capacity. Interestingly, a DSC-crosslinking simulation experiment performed after four months from electrospinning (Figure S3b in SI), shows that CH/CS scaffold evolution occurs also in the non-crosslinked state, as it was detected by SAXS in its crosslinked-hydrated state. The structural evolution is parallel to a modification of embedded water activity. This shows as a typical feature of the blend, which might be exploited if shorter-time membrane degradation is needed.

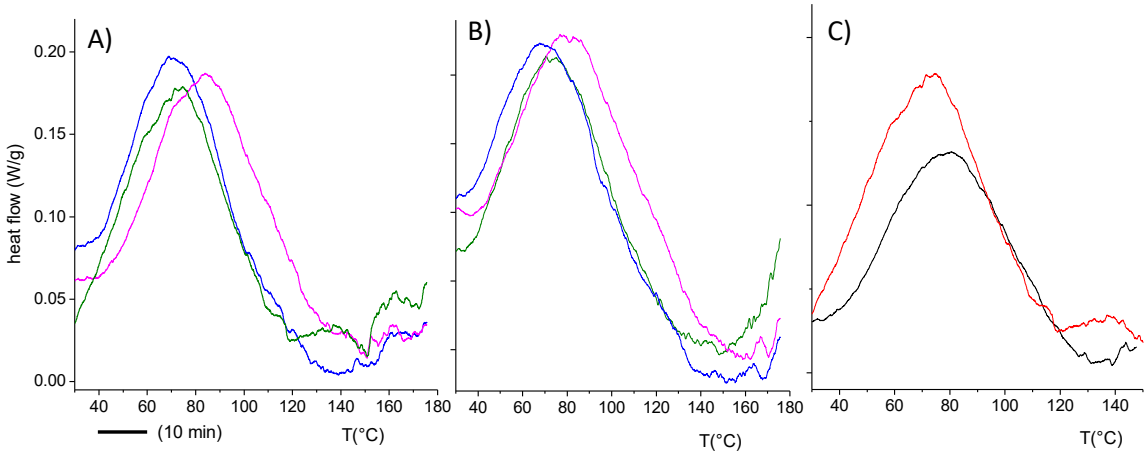

348

349 FIGURE 5. A) DSC of the crosslinked scaffolds, with a 2°C/min heating scan. The time scale is reported, color
350 code as in Fig. 4. B) DSC of the DSC-simulated crosslinked scaffolds, after two weeks, with a 2°C/min heating
351 scan. C) DSC of non-crosslinked (black) and crosslinked (red) CH scaffold.

352

353 3.2.5. Surface zeta potentials

354 Figure 6 shows the pH dependence of the ζ for the cross-linked scaffolds. The reference material is either
355 PVDF or a silicon wafer with a SiO_2 top layer as indicated in the legend. The isoelectric points (iep) of the
356 scaffolds are given in the inset.

357 The evolution of the apparent ζ with the pH of the aqueous 0.01 mol/l KCl solution show similar trends for CH
358 and CH/CS scaffolds (iep at pH 2.7 ± 0.1 and at pH 2.9, respectively) and a plateau above pH 5, showing the
359 substantial effect of CA in the CH scaffold. Nonetheless, the measured plateau values of ζ are significantly
360 different for CH and CH/CS (ζ = –17.2 ± 2.0 mV; ζ = –13.8 ± 0.9 mV, respectively), indicating that their
361 electric behavior at the scaffold-water interface is not the same.

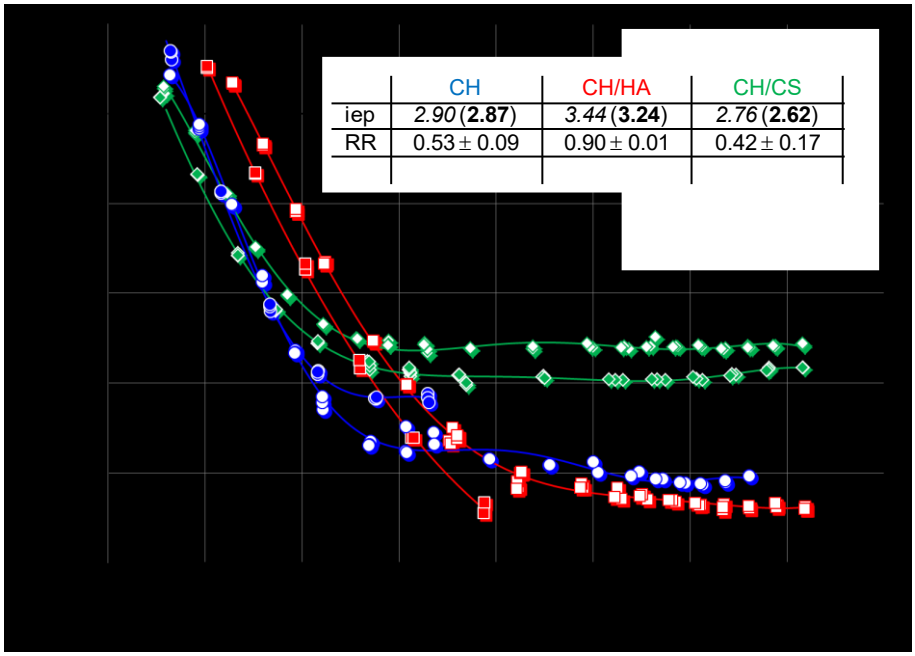

FIGURE 6: zeta potential vs pH profiles obtained for cross-linked CH (blue), CH/CS (green) and CH/HA (red) scaffolds. In the inset, the isoelectric points (iep) of scaffolds with the two reference materials, PVDF (*italics,* full symbols) and SiO_2 (**bold**, void symbols) and the ratio RR between measured and expected Ohm resistances in the flow channel. The PVDF and SiO_2 iep are 4.02 and 3.59, respectively (SI).

The CH/HA scaffold displays a markedly different pH-dependence of ζ, with an iep at higher pH (pH_{iep} 3.3 ± 0.1) and a less pronounced ζ-plateau, and only at pH > 7.5, a steady value of ζ = –22 mV is reached. Merging the information about the iep and the magnitude of the ζ in the plateau region, the three scaffolds could be differentiated in terms of the surface and interfacial charge. All the three scaffolds have negative zeta potential in physiological fluids, stemming for a non-negligible impact of CA 1:1 in weight ratio to chitosan, otherwise expected to show a much higher iep. However the different behavior of the three scaffolds, considering iep and ζ at plateau regions, could be related to the strong interaction between CS and the amino groups of CH that could compete with CH-CA interaction, while the interaction between CH and HA is conceivably weaker considering the lower acidity of the carboxylic groups of HA as compared to the sulfate groups of CS. Combined measurement of streaming potential and streaming current (detailed in SI) allowed estimating the ratio (RR, Fig 6, inset) of the effective and electrolyte resistances (RR). CH and CH/CS scaffolds are characterized by similar low values of RR (0.53 ± 0.09 and 0.42 ± 0.17, respectively), which indicate a significant effect of swelling. The RR value close to unity (0.90 ± 0.01) for CH/HA suggests that this shows a smaller swelling propensity. The apparently contrasting information about the swelling propensity of the different scaffolds as determined by microscopy, SAXS and ζ, shows that swelling occurred

384 at different scales. In fact, it appears that in the CH/HA scaffold swelling is sustained by single fibers, while in
385 the CH and CH/CS, it is due to dilatation of the scaffold mesh.
386
387 3.2.6. Mechanical properties
388 Both dry and hydrated cross-linked scaffolds were tested for tensile strength TS (N/cm^2) and elongation (E%)
389 at break point (Fig. S5, SI). All scaffolds display higher TS and lower E% in dry rather than wet state (both
390 parameters, by roughly one order of magnitude). When dry, CH/CS TS value is roughly half than for CH and
391 CH/HA, with similar elongation. In the hydrated state, this feature is more evident, as, although showing
392 similar values of force at break, CH/CS scaffold shows significantly higher values for E%, roughly doubling its
393 length before breaking, about 20% higher than the CH scaffold and twice that of CH/HA. Then, the presence
394 of CS conceivably improves the ability of the scaffold to be deformed without breaking.
395
396 3.3. Biopharmaceutical characterizations
397 3.3.1. In vitro cell adhesion and proliferation assay: fibroblasts and endothelial cells
398 In Figure S6 cytotoxicity results are shown and fibroblasts and HUVEC viability (optical density, OD)
399 evaluated for cells grown onto CH, CH/CS and CH/HA scaffolds and in standard conditions (GM, cells grown
400 directly on plastic well bottom was considered as standard growth) for 3 and 6 days is reported (SI).
401 Independently of the cell type there is an increase in cell population grown onto scaffolds from 3 to 6 days to
402 indicate that the scaffolds support the cell growth along time without impairing their proliferation and no
403 difference between GM and scaffolds could be evidenced.
404 While after 6 days fibroblasts proliferate much more onto CH/CS scaffolds while CH scaffolds is
405 characterized by lower cell proliferation than GM. In the case of HUVEC, scaffolds allow a cell growth like
406 GM: CH/HA determined a cell growth higher than those of the other scaffolds and CH/CS showed a slightly
407 lower cell proliferation with respect to CH/HA.
408 Figure 7 reports SEM and CLSM of fibroblasts (a) and HUVEC (b) grown onto scaffolds for 6 days (the 3
409 days growth is shown in Fig. S7). These analyses confirm the proliferation results (viability). SEM
410 microphotographs evidence that cells grow in an intimate contact with the scaffold structure and the
411 nanofibers appear integrated in the cell substrates at subconfluency. CLSM put in evidence that fibroblasts
412 grown onto the scaffolds are characterized by normal fusiform shapes and aligned cytoskeletons while
413 HUVEC cells present polygonal shape. CH and CH/CS scaffolds seem to better allow cell adhesion and
414 proliferation showing greater number of cells.

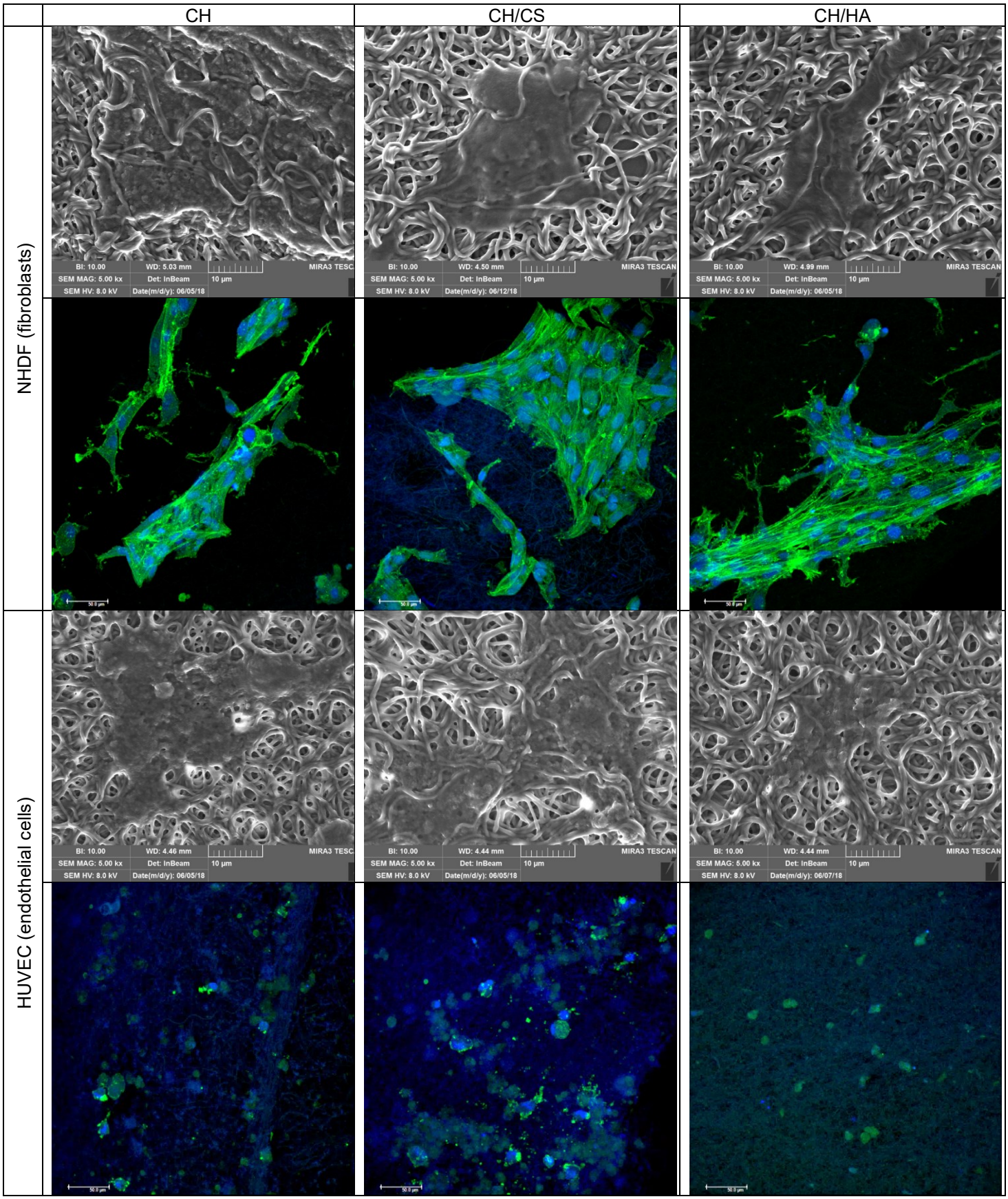

415 FIGURE 7: SEM and CLSM (in blue the nuclei and in green the cytoskeleton) microphotographs of
416 fibroblasts (NHDF) and endothelial cells (HUVEC) grown onto CH (left), CH/CS (centre) and CH/HA (right)
417 scaffolds for 6 days.

418 3.3.2. In vivo wound healing efficacy in rat model

419 Figure 8 shows lesion area vs time of treatments and the histology in correspondence of the lesions after 18
420 days of treatment with CH, CH/CS and CH/HA scaffolds in an in vivo murine burn/excisional model. Intact
421 skin (positive reference) and skin section in correspondence to the lesion after 18 days of treatment with
422 saline solution (negative reference) are also reported.

423 Lesions treated with CH/CS, CH and CH/HA are in a more advanced stage of wound healing as compared to
424 samples treated with saline solution (Fig. 8 B), in which there is a large part of skin surface without
425 epithelium. Furthermore, in saline-treated lesions, the underlying connective tissue is still affected by an
426 abundant inflammatory infiltrate, with numerous dilated vessels, while collagen fibers are dispersed and not
427 yet organized. All the scaffolds can improve the skin recovery as compared to the reference although there
428 are differences in scaffold performance. CH/CS appears to be the best performing of the three (Fig. 8 D).
429 The epidermal layer appears fully restored, thick and well organized in several cell layers, and shows a fair
430 degree of keratinization (cornification). Inflammatory infiltrate is almost completely absent, as well as
431 abnormally dilated vessels. A fine network of collagen fibers is restored at the dermo-epidermal junction and
432 the bundles of collagen fibers in the dermis has a normal size.

433 CH scaffold (Fig. 8 C) shows full restoration of the epidermal layer, thick and fairly keratinized. Bundles of
434 collagen fibers of normal size are restored at the wound edges. But the dermis in the injured area is still
435 rather infiltrated by inflammatory cells with several dilated vessels. Finally, also the CH/HA scaffold (Fig. 8
436 E) displays a suboptimal performance with the epidermal layer not fully restored, and necrotic material
437 detectable over the lesion. The dermis in the injured area is infiltrated by several inflammatory cells with
438 dilated vessels.

439 In all cases the histologic analysis does not show any residues of the scaffolds. This could be probably due
440 to enzymatic degradation caused by lysozyme, which chitosan is a substrate of. In fact lysozyme is normally
441 secreted by white cells recruited in the lesion bed during the inflammatory phase of the healing process.

442

443

444

445

446

447

448

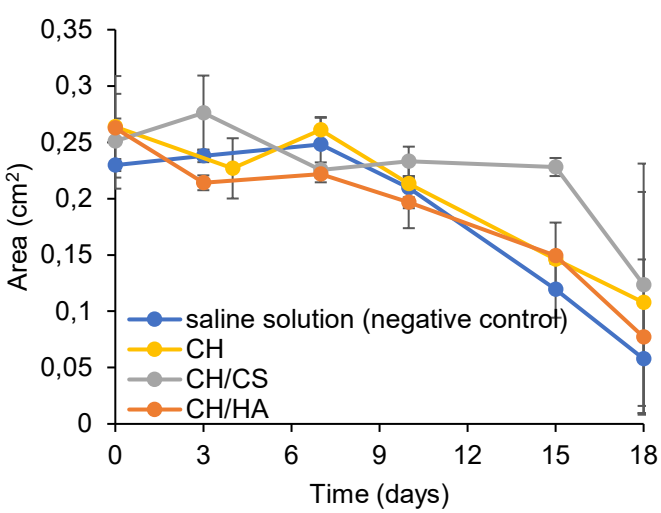

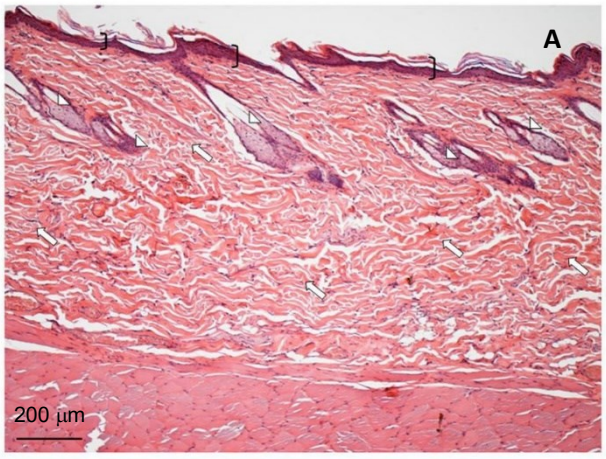

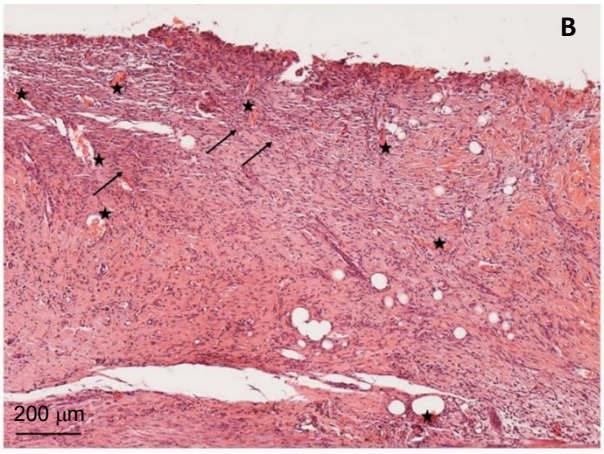

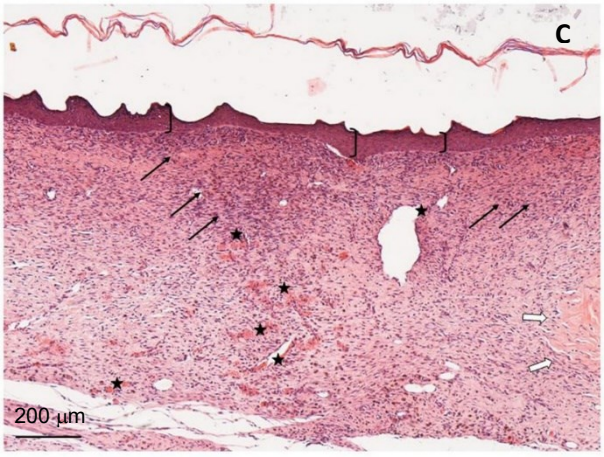

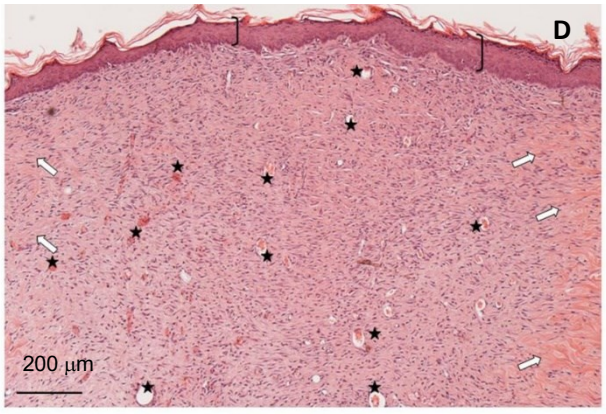

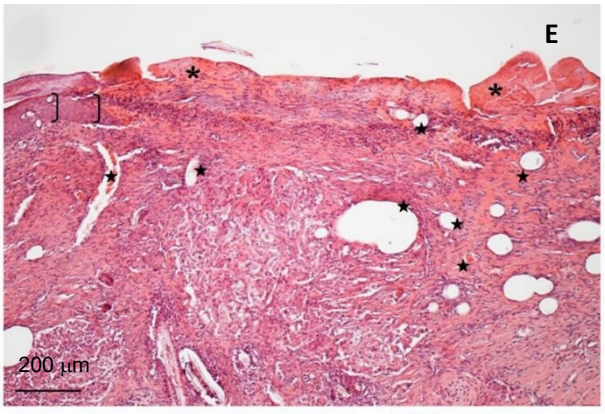

FIGURE 8: lesion area vs time obtained during the treatments using CH, CH/CS and CH/HA scaffolds in an in vivo murine burn/excisional model (mean values±sd; n=3) and H&E sections of A) intact skin; B) lesion treated with CH scaffold; C) lesion treated with CH/CS scaffold; D) lesion treated with CH/HA scaffold; E) V lesion treated with saline solution as negative control (scale bars are 200 μm).

Conclusions

Electrospinning was successfully used to prepare scaffolds for reparation of critical skin lesions, like burns. The developed process allowed to obtain nanofibrous membranes entirely based on polysaccharides, starting from aqueous polymer blends. Polymers with opposite charges (CH, cationic, and CS or HA, anionic) could be simultaneously electrospun with P as matrix-forming polysaccharide. CA, present in the polymer blends, was added as cross-linking agent and activated by heating.

The nanofibers show regular shape and smooth surface, preserved upon the cross-linking process. The resistance of scaffolds to solubilization in aqueous fluids seems attributable to two phenomena occurring at crosslinking heat treatment: the creation of amide bonds (mainly in the CH scaffold, while hindered by the formation of PEC in CH/CS and CH/HA scaffolds) and felting, occurring when water is released from the electrospun scaffold, resulting in local physical multi-entanglement between fibers, that could not be released by simple hydration. Nonetheless, the water holding capacity of the scaffolds is preserved, and conceivably increased, by crosslinking,

CH/CS scaffold shows the best performance in allowing the skin healing in vivo (murine burn/excisional model) and correspondingly, it evidences the best proliferation properties in vitro (fibroblasts and HUVEC). The physico-chemical analysis suggests that the CH/CS scaffold offers more adaptability in terms of swelling and fiber roughening once hydrated, thus conceivably allowing for optimal cell adhesion and migration, moreover profiting from the CS protrusion/release from the fibers. In addition, the macroscopic feature of a pronounced deformability pointed at the CH/CS scaffold as a good protective cover for non-flat or irregular surfaces.

Acknowledgements

The authors thank M. Sztucki for assistance on ID02 (ESRF, Grenoble) and the partnership for Soft Condensed Matter (PSCM, ILL/ESRF, Grenoble) for use of in-house facilities.

Funding

This research did not receive any specific grant from funding agencies in the public, commercial, or not-for-profit sectors.

Data availability

The raw and processed data required to reproduce these findings cannot be shared at this time as part of an ongoing study. In the SI supplementary findings support the results obtained.

REFERENCES

Feng, F., Liu, Y., Zhao, B., Hu, K. (2012) Characterization of half N-acetylated chitosan powders and films, *Procedia Engineering*, 27, 718-732.

Goldberg, M., Langer, R., Jia, X. (2012) Nanostructured materials for applications in drug delivery and tissue engineering, *Journal of Biomaterials Science Polymer edition*, 18, 241-268.

Harish Prashanth, K.V., Kittur, F.S., Tharanathan, R.N. (2002) A physico-chemical comparative study on extracellular carbohydrate polymers from five desert algae, *Carbohydrate Polymers*, 50, 27-32.

Huan, S., Liu, G., Han, G., Cheng, W., Fu, Z., Wu, Q., Wang, Q. (2015) Effect of Experimental Parameters on Morphological, Mechanical and Hydrophobic Properties of Electrospun Polystyrene Fibers. *Materials*, 8, 2718 -2734

Kim, H., Jeong, H., Han, S., Beack, S., Hwang, B. W., Shin, M., Oh, S. S., Hahn, S. K. (2017) Hyaluronate and its derivatives for customized biomedical applications, *Biomaterials*, 123, 155-171.

Kupiec, T.C., Matthews. P., Ahmad, R. (2000) Dry-heat sterilization of parenteral oil vehicles. *International Journal of Pharmaceutical Compounding,* 4, 223-4.

Liu, H., Wang, C., Li, C., Qin, Y., Wang, Z., Yang, F., Li, Z., Wang, J. (2018) A functional chitosan-based hydrogel as a wound dressing and drug delivery system in the treatment of wound healing, *RSC Advances,* 8 7533-7549.

Liu, M., Duan, X.-P., Li, Y.-M., Yang, D.-P., Long. Y.-Z. (2017) Electrospun nanofibers for wound healing, *Materials Sciences and Engineering C*, 76, 1413-1423.

Luxbacher, T. (2014) The ZETA Guide – Principles of the streaming potential technique, Anton Paar GmbH, ISBN 978-3-200-03553-9

Mafazzal Jahromi, M.A., Sahandi Zangabad, P., Moosavi Basri, S.M., Sahandi Zangabad, K., Ghamarypour, A., Aref, A.R., Karimi, M., Hamblin, M.R. (2018) Nanomedicine and advanced technologies for burns: Preventing infection and facilitating wound healing, *Advanced Drug Delivery Reviews*, 123, 33-64.

Oliveira, J. T., Reis, R. L.J. (2011) Polysaccharide-based materials for cartilage tissue engineering applications, *Tissue Engineering and Regenerative Medicines*, 5, 421 -36.

Pedersen, J. S. (1997) Analysis of small-angle scattering data from colloids and polymer solutions: modeling and least-squares fitting *Advances in Colloid and Interface Sciences*, 70, 171-210

546 Qasim, S.B., Zafar, M.S., Najeeb, S., Khurshid, Z., Shah, A.H., Husain, S., Rehman I. U. (2018)
547 Electrospinning of Chitosan-Based Solutions for Tissue Engineering and Regenerative Medicine,
548 *International Journal of Molecular Sciences*, 19, 407.
549 Sandri, G., Bonferoni, M. C., Rossi, S. Ferrari, F., Mori, M., Cervio, M., Riva, F., Liakos, I., Athanassiou, A.,
550 Saporito, F., Marini, L., Caramella, C. (2015) Platelet lysate embedded scaffolds for skin regeneration,
551 *Expert Opinion on Drug Delivery*, 12, 525-545. https://doi.org/10.1517/17425247.2015.961421.
552 Sandri, G., Bonferoni, M. C., Rossi, S., Delfino, A., Riva, F., Icaro Cornaglia, A., Marrubini, G., Musitelli, G.,
553 Del Fante, C., Perotti, C., Caramella, C., Ferrari, F. (2016) Platelet lysate and chondroitin sulfate loaded
554 contact lenses to heal corneal lesions, *International Journal of Pharmaceutics*, 509, 188-196.
555 Sandri, G., Bonferoni, M. C., Rossi, S., Ferrari, F., Mori, M., Del Fante, C., Perotti, C., Caramella, C. (2012)
556 Thermosensitive eyedrops containing platelet lysate for the treatment of corneal ulcers *International Journal*
557 *of Pharmaceutics*, 426, 1-6.
558 Saporito, F., Sandri, G., Rossi, S., Bonferoni, M.C., Malavasi, L., Del Fante, C., Vigani, B., Black, L., Ferrari,
559 F. (2018a) Electrospun gelatin–chondroitin sulfate scaffolds loaded with platelet lysate promote immature
560 cardiomyocyte proliferation. *Polymers*, 10, 208.
561 Saporito, F., Sandri, G., Rossi, S., Bonferoni, M.C., Riva, F., Malavasi, L., Caramella, C., Ferrari, F. (2018b)
562 Freeze dried chitosan acetate dressings with glycosaminoglycans and traxenamic acid, *Carbohydrate*
563 *Polymers*, 184, 408-417.
564 Singh, R.S., Kaur, N., Rana, V., Kennedy, J.F. (2017) Pullulan: A novel molecule for biomedical applications
565 *Carbohydrate Polymers*, 171, 10-121.
566 Stejskalova, A., Almquist, B.D. (2017) Using biomaterials to rewire the process of wound repair, *Biomaterials*
567 *Science*, 5, 1421- 1434.
568 Walker, S. L., Bhattacharjee, S., Hoek, E. M. V., Elimelech, M. (2002) A Novel Asymmetric Clamping Cell for
569 Measuring Streaming Potential of Flat Surfaces. *Langmuir,* 18, 2193 –2198. DOI: 10.1021/la011284j
570 Yamada, S., Sugahara, K. (2008). Potential therapeutic application of chondroitin sulfate/dermatan sulfate,
571 *Current Drug Discovery. Technologies*, 5, 289-301
572 Yamaguchi, I., Tokuchi, K., Fukuzaki, H., Koyama, Y., Takakuda, K., Monma, H., Tanaka, J. (2001)
573 Preparation and microstructure analysis of chitosan/hydroxyapatite nanocomposites, *Journal of Biomedical*
574 *Material Research*, 55, 20-27.